Nonstationary warm spell frequency analysis integrating climate variability and change with application to the Middle East

Taha B.M.J. Ouarda[1, 4, *], Christian Charron[1], Kondapalli Niranjan Kumar[2], Devulapalli Venkata Phanikumar[3], Annalisa Molini[4] and Ghouse Basha[5]

[1]Canada Research Chair in Statistical Hydro-Climatology, INRS-ETE, National Institute of Scientific Research, Quebec City (QC), G1K9A9, Canada

[2]Physical Research Laboratory, Ahmedabad, India

[3]Department of Science and Technology, Ministry of Science and Technology, Technology Bhawan, New Delhi

[4]Institute Center for Water and Environment (iWATER), Masdar Institute of Science and Technology, P.O. Box 54224, Abu Dhabi, UAE

[5]National Atmospheric Research Laboratory, Department of Space, Gadanki-517112, India

*Corresponding author:

Email: taha.ouarda@ete.inrs.ca

Tel: +1 418 654-3842

April 2019

Abstract

The Middle East can experience extended wintertime spells of exceptionally hot weather, which can result in prolonged droughts and have major impacts on the already scarce water resources of the region. Recent observational studies point at increasing trends in mean and extreme temperatures in the Middle East, while climate projections seem to indicate that, in a warming weather scenario, the frequency, intensity and duration of warm spells will increase. The nonstationary warm spell frequency analysis approach proposed herein allows considering both climate variability through global climatic oscillations and climate change signals. In this study, statistical distributions with parameters conditional on covariates representing time, to account for temporal trend, and climate indices are used to predict the frequency, duration and intensity of wintertime warm spells in the Middle East. Such models could find a large applicability in various fields of climate research, and in particular in the seasonal prediction of warm spell severity. Based on previous studies linking atmospheric circulation patterns in the Atlantic to extreme temperatures in the Middle East, we use as covariates two classic modes of 'fast' and 'slow' climatic variability in the Atlantic Ocean (i.e., the Northern Atlantic Oscillation (NAO) and the Atlantic Multidecadal Oscillation (AMO) respectively). Results indicate that the use of covariates improves the goodness-of-fit of models for all warm spell characteristics.

Keywords: Winter warm spell; Nonstationary model; Frequency analysis; Climate index; Climate change; Natural climate variability; Statistical distribution; Middle East.

1. Introduction

In the recent years, an important number of heat waves have been observed around the world resulting in severe adverse societal and economic impacts (Ouarda and Charron, 2018). Examples include Chicago in 1995 (Karl and Knight, 1997), Europe in 2003 (Garcia-Herrera et al., 2010), Greece in 2007 (Founda and Giannakopoulos, 2009), Australia in 2009 (Karoly, 2009), Russia in 2010 (Dole et al., 2012) and Eastern China in 2013 (Sun et al., 2014). While the most immediate adverse impacts of extreme temperatures are those on human health, adverse impacts on natural ecosystems are also important: extreme temperatures and prolonged dry spells induce significant water stress, which brings long-term consequences on vegetation development (Gobron et al., 2005). A number of studies have reported increases in extreme temperature indices since the middle of the 20th century (Alexander et al., 2006; Brown et al., 2008; Perkins et al., 2012; Coumou et al., 2013). It has been argued in several studies that the increase in the reported extreme events is a consequence of global warming (Coumou and Robinson, 2013) which is about 0.5-0.6°C globally since 1951-1980 (Hansen et al., 2012). Many studies point out that, in a context of climate change, the frequency, intensity and duration of extreme heat waves are likely to increase in the future based on climate change scenarios (IPCC, 2012; Coumou and Rahmstorf, 2012; Coumou et al., 2013; Russo et al., 2014; Basha et al., 2017).

The Middle East, one of the world most water-stressed regions, is especially sensitive to global warming. The majority of studies on the evolution of climate extremes in the Middle East concluded to an increase in temperature extreme indices and a decrease in precipitation extreme indices during the recent decades (Ouarda et al., 2014). Future climate projections seem also to support an increasing trend in heat extremes over the Middle East. Lelieveld et al. (2016), for example, pointed up a consistent positive trend in warm extremes over the region in the CMIP5 ensemble models, for both the RCP4.5 and RCP8.5 (business as usual) scenarios.

Most of the studies analyzing the extreme temperature regime in the Middle East focus on summer extreme temperatures, due to their immediate impacts on population health (Masselot et al., 2018). However, winter warm spells have also important health, hydrological and environmental impacts. They seriously enhance evapotranspiration and reduce potential groundwater recharge over the water stressed region of the Middle East. Gonzalez et al. (2016) showed that low rainfall, economic and population growth and agricultural development resulted in a dramatic depletion of groundwater resources in the United Arab Emirates (UAE) region during the period 2003-2012. In the context of rapid growth and scarcity of water resources, the Middle East is particularly vulnerable to future climate change (Evans, 2010). Given the evidence of an increasing trend in the observed frequency of occurrence of hot temperature extremes and the projected climate change in the future (IPCC, 2007), the impacts of extreme temperatures have become a growing concern for the Middle East especially during the wet winter season.

The study of the physical mechanisms behind heatwaves has been a topic of increased interest (Horton et al., 2016). Perkins (2015) reviewed the physical mechanisms driving heatwaves and identified three major mechanisms. The first one is the presence of a high-pressure synoptic system which results in a stationary system that remains over an area for an abnormally long period. Another driving mechanism is related to the coupling of atmosphere and land surface. Indeed, interactions between air temperature and soil moisture result in important summer temperature variability. The third driving mechanism is associated to climate variability and large-scale teleconnections which influence extreme temperatures at a global scale.

Large scale oscillation patterns have a preponderant influence on the climate of the Middle East. Kumar et al. (2017) demonstrated that the Atlantic and Mediterranean SSTs have a significant influence on winter warm spells over the region. The authors stated that “large and persistent Atlantic SST anomalies modulate the occurrence of the winter warm spells in the Middle East at interannual and decadal scales through the mediation of the Mediterranean SSTs, creating the conditions for the development of extended and persistent anticyclonic structures over the region”. The link between circulation modes and the Middle East climate has been established in many studies (Türkeş and Erlat, 2003; Folland et al., 2009; Erlat and Türkeş, 2013; Donat et al., 2014).

The Northern Atlantic Oscillation (NAO) is the most frequent mode reported to have an influence on the region (Mann, 2002; Marshall et al., 2001; Cullen et al., 2002; Chandran et al., 2016; Naizghi and Ouarda, 2017). The impacts of this pattern are known to be much stronger during the winter season (Marshall et al., 2001; Cullen et al., 2002). Wetter and cooler conditions than normal in the Middle East are associated with positive phases of NAO while drier and warmer than normal conditions are associated with negative phases (Cullen and deMenocal, 2000). Persistent positive values of NAO observed since 1980 may have masked the influence of anthropogenic climate change in the region in recent decades (Mann, 2002). Kumar et al. (2017) also observed that the decadal trends in the occurrence and duration of winter warm spells in the Middle East are significantly correlated with the Atlantic Multidecadal Oscillation (AMO).

The influence of other atmospheric circulation indices seems to be less important. The El Niño–Southern Oscillation (ENSO) phenomenon, known to have important impacts on climate around the world, is reported to have a weak influence on temperatures in the region (Halpert and Ropelewski, 1992; Karabörk et al., 2005). However, ENSO is reported to have a significant impact on the precipitations in the Arabian Peninsula (Ouarda et al., 2014; Niranjan Kumar et al., 2016), although mainly in terms of moisture advection and precipitable water availability.

Statistical methods based on extreme value theory have been used extensively in the analysis of hydrological and weather extremes (Katz et al., 2002; El Adlouni et al., 2007; Ouarda et al., 2019). They have been recently applied to heat waves and warm spells (Furrer et al., 2010; Khaliq et al., 2011; Keellings and Waylen, 2014, 2015; Katz and Grotjahn, 2014; Photiadou et al., 2014; Abaurrea et al., 2015). Traditionally, stationarity in time series is assumed and static probability distributions are used. However, in the context of climate warming and under the influence of large scale oscillation patterns, weather extremes are not stationary. One approach to deal with nonstationarity in data samples is to introduce covariates into the parameters of the distribution (e.g. Strupczewski at al., 2001; Khaliq et al., 2006; Ouarda and El Adlouni, 2011). Such distributions are termed conditional because they depend on time-dependent covariates. Such covariates could incorporate trends, cycles or physical variables that can represent atmosphere-ocean patterns (Katz et al., 2002; Hundecha et al., 2008). Conditional distributions with a covariate representing the year were extensively used for trend analysis in climate extremes (Kharin and Zwiers, 2005; Brown et al., 2008; Laurent and Parey, 2007; Parey et al., 2007; Keellings and Waylen, 2014). Conditional distributions were also used with climate indices of atmospheric circulation as covariate to evaluate the statistical significance of the influence of large scale atmospheric patterns on climate extremes (Sillmann et al., 2011; Photiadou et al., 2014; Keellings and Waylen, 2015; Grotjahn et al., 2016).

In general, models with parameters that are conditional on climate indices may find applications in a number of fields where conditional risk management is required. The severity of warm spells could be predicted for the next season based on actual information about the covariates and can help managers with the decision making process. Predictions of warm spell severity could be of interest for managers in various fields including agriculture (Crane et al., 2011), health care (Ebi et al., 2006; Patz et al., 2000; Bayentin et al., 2010) and hydrology (Pulwarty and Melis, 2001). It is also possible to predict climate indices in the near future (Sutton et al., 2000; Lee and Ouarda, 2011). Climate forecasting was proven in Jones et al. (2000) to be beneficial for agriculture with decisions conditioned on ENSO phases. A climate forecast information system based on ENSO was developed in the southeastern USA for the management of risk in the field of agriculture (Fraisse et al., 2006). Lowe et al. (2011) reported that heatwave early warning systems have been implemented in 12 European countries to reduce the impacts on public health.

In this study, we propose to model the frequency, duration and intensity of wintertime warm spells in the Middle East using nonstationary statistical models with parameters that are conditional on diverse climatic covariates. This approach allows us to account for the effects of global warming and large-scale climate oscillation patterns. The aim of this study is to assess the statistical significance of recent trends caused by both anthropogenic and internal climate variability on wintertime warm spells in the Middles East. Two important climate indices in the Atlantic known to have an influence on wintertime weather patterns in the Middle East, the NAO and the AMO, are used as covariates. The year is used as an additional covariate to represent the temporal trend. Analyses are performed on the regional averaged maximum temperature over a homogenous region in the Middle East. Such approach has never been applied to model climate extremes, including warm spell indices, in the Middle East. While nonstationary models for warm spells have been applied in other regions, models integrating both climate indices and a temporal trend have never been applied.

2. Methods

2.1 Statistical modeling of warm spells

2.1.1 Modelling of the intensity and frequency

In extreme value theory, one approach that has received large popularity consists in extracting the most extreme value within a season and is termed block maxima (BM). Under a wide range of conditions, the distribution of BM can be approximated by the generalized extreme value (GEV) distribution (Coles, 2001). The cumulative distribution function of the GEV is defined by:

$$GEV(x;\mu,\alpha,\kappa)=\begin{cases}\exp\left[-\left(1+\dfrac{\kappa}{\alpha}\left(x-\mu\right)\right)^{-1/\kappa}\right], & \kappa\neq 0\\ \exp\left[-\exp\left(-\dfrac{\left(x-\mu\right)}{\alpha}\right)\right], & \kappa=0\end{cases} \qquad (1)$$

where μ, $\alpha > 0$ and κ are the location, scale and shape parameters respectively, and $\mu-\alpha/\kappa<x<\infty$ for $\kappa>0$, $-\infty\leq x\leq+\infty$ for $\kappa=0$ and $-\infty\leq x\leq u-\alpha/\kappa$ for $\kappa<0$.

Another approach, termed peak-over-threshold (POT), consists in extracting exceedances over a sufficiently high threshold. This approach is more appropriate for the analysis of the warm spells in this study because they represent events over a high threshold. An advantage of this approach is that the upper tail of the distribution can be better sampled since more events can be considered during a given season, instead of limiting the sampling to only one peak as in the case of the BM approach (Lang et al., 1999). Another advantage is that the two extreme event components, the rate of occurrence and the intensity of exceedances over the threshold can be modeled separately. The rate of occurrence of rare events is generally modeled by a Poisson(POI) distribution as justified by the law of small numbers, while the intensity of exceedances over a sufficiently high threshold is generally modeled by a Pareto (GP) distribution as justified by the theory of extreme values (Ashkar and Ouarda, 1996; Katz and Grotjahn, 2014). This consists in the POI-GP model where intensity and frequency are modeled separately with POI and GP respectively (Katz et al., 2002).

The cumulative distribution function of the GP is defined by:

$$GP(x;u,\sigma,\kappa)=\begin{cases}1-\left(1+\dfrac{\kappa}{\sigma}\left(x-u\right)\right)^{-1/\kappa}, & \kappa\neq 0\\ 1-\exp(-\dfrac{x-u}{\sigma}), & \kappa=0\end{cases} \tag{2}$$

where u, $\sigma > 0$ and κ are the threshold, scale and shape parameters respectively, $u<x<u-\sigma/\kappa$ for $\kappa<0$, $x\geq u$ for $\kappa\geq 0$. The parameter σ depends on the threshold and is linked to the parameters of the corresponding GEV distribution by the relation:

$$\sigma=\alpha+\kappa(u-\mu). \tag{3}$$

The probability mass function of the POI distribution is defined by:

$$Poi(N=n;\lambda)=e^{-\lambda}\lambda^{n}/n!,\quad n=1,2,\ldots. \tag{4}$$

where $\lambda > 0$ is the rate parameter and N is the number of crossings of the threshold u.

2.1.2 Modelling of the duration

It is also common to model the warm spell duration. In a number of studies, the durations of the warm spells were modeled with a geometric distribution (Furrer et al. 2010; Modal and Mujumdar, 2015; Keellings and Waylen, 2014; Wang et al., 2015). The probability mass function of the zero-truncated geometric distribution (GEO) is defined by:

$$Geo(K=k;p)=(1-p)^{k-1}p, \quad k=1,2,\ldots \tag{5}$$

where 1/p is the mean duration and K is the length of the warm spell.

2.2 Nonstationary models

In nonstationary models, distribution parameters are made conditional on time-dependent covariates. The relations between distribution parameters and covariates can take the form of simple linear combinations (El Adlouni et al., 2007; El Adlouni and Ouarda, 2009) or more complex models such as B-splines (Nasri et al., 2013; Thiombiano et al., 2017). When the POI-GP model is adopted, usually, the scale parameter (σ) of the GP is made conditional on covariates, the shape parameter (κ) of the GP is kept constant, and the rate parameter (λ) of the POI is made conditional on covariates (Kysely et al., 2010; Modal and Mujumdar, 2015; Thiombiano et al., 2018). In this study, the logarithm of the rate parameter λ in POI can depend linearly or quadratically on a given time-dependent covariate Y_t:

$$\ln(\lambda_t)=\beta_0+\beta_1 Y_t \text{ or } \ln(\lambda_t)=\beta_0+\beta_1 Y_t+\beta_2 Y_t^2 \tag{6}$$

where β are parameters to be estimated. Logarithmic transformations are used to ensure a positive value of the distribution parameters. For GP, the logarithm of the scale parameter can depend linearly or quadratically on the time-dependent covariate Y_t:

$$\ln(\sigma_t)=\beta_0+\beta_1 Y_t \text{ or } \ln(\sigma_t)=\beta_0+\beta_1 Y_t+\beta_2 Y_t^2. \tag{7}$$

For GEO, the logarithm of the location parameter can depend linearly or quadratically on the time-dependent covariate Y_t:

$$\ln(p_t) = \beta_0 + \beta_1 Y_t \text{ or } \ln(p_t) = \beta_0 + \beta_1 Y_t + \beta_2 Y_t^2 . \tag{8}$$

The cases of conditional distributions with 2 and 3 covariates are also considered. Given two additional covariates Z_t and W_t, different combinations of linear and quadratic dependence relationships between the distribution parameter (λ_t, σ_t or p_t) and the covariates Y_t and/or Z_t are considered.

Three main covariates are used in the nonstationary case: 'fast' (subdecadal) and 'slow' (multidecadal) climate indices (i.e., NAO and AMO respectively), and Time (represented by the year). The wintertime (NDJFM) averages of NAO and AMO are computed and used as covariates to model the frequency of the winter warm spells. Time is defined by a series of integers incremented from 1 to the number of years in the series, to model the frequency. For the duration and the intensity, each event can be identified precisely in time and thus more precise months can be used to compute the covariates NAO and AMO. A simple method used here consists in taking the average for the three-month period centered on the date of the maximum intensity of each warm spell. Time for the duration and intensity is considered fixed over the warm spell season within a given year but is allowed to shift from one year to another.

2.3 Parameter estimation

For a given model, the vector of the distribution parameters β is estimated with the maximum likelihood method (ML). For a given probability distribution *f*, the likelihood function for the sample $x = \{\mathrm{x}_1, ..., \mathrm{x}_n\}$ is given by:

$$L_n = \prod_{t=1}^{n} f(x_t; \beta) . \tag{9}$$

Hence, $\hat{\beta}$ is the estimator of β that maximizes the likelihood function L_n.

2.4 Model selection and comparison

To select the complexity of a model with given covariates, the deviance statistic can be used for model selection as proposed by Coles (2001). Suppose two models M_1 and M_0, where M_0 is a subset of M_1. The deviance statistic is defined by:

$$D = 2\{\ell_1(M_1) - \ell_0(M_0)\} \tag{10}$$

where $\ell_1(M_1)$ and $\ell_0(M_0)$ are the maximized values of the log-likelihood for models M_1 and M_0 respectively. It can be proven that D is distributed according to the χ_l^2 distribution where l is the difference between the dimension of M_1 and M_0. A test of validity of the model M_0 relative to M_1 is to reject M_0 in favor of M_1 if $D > \chi_l^2$ for a given level of significance.

To compare the goodness-of-fit of different models, we use the Akaike information criterion (AIC), defined as:

$$\mathrm{AIC} = -2\ln(L_n) + 2d\,, \tag{11}$$

where d is the number of parameters of the model or the length of the vector θ. This statistic accounts for the goodness-of-fit of the model and also for the parsimony through the parameter k whose value increases with model complexity.

2.5 Definition of warm spells

There is in general very little consensus and consistency in the literature on how to identify warm spells, and different studies often rely on very different definitions and selection thresholds

(Perkins and Alexander, 2012; Masselot et al., 2018). The simplest definition is ‘the period of consecutive days with temperature over a given relative or absolute threshold’, which, however, risks to marginalize the role of local climatology (Robinson, 2001). In this study we follow a percentile based criterion similar to the ones proposed by Della-Marta et al. (2007) and Stefanon et al. (2012), where a heat wave is defined as the period of consecutive days where the daily maximum temperature exceeds the long-term (climatological) 90th percentile of daily maximum temperatures. For each day of the year, a 90th percentile is calculated from a sample of 15 days centered on the considered day using data over the whole base period. This is equivalent to the POT approach with a relative threshold dependent on the day of the year. Also, we introduce the additional constraint that both daily maximal and minimal temperatures should exceed the daily maximum and minimum temperatures 90th percentiles. A minimum number of days above the threshold may be considered (e.g. Freychet et al., 2018) or not (Furrer et al., 2010). In this study, a minimum duration is not considered. Declustering is frequently used with the POT approach to avoid consecutive dependent events. A common rule to separate exceedances in clusters is to consider clusters separated by r consecutive values below the threshold as independent (Coles, 2001). The choice of r is arbitrary: a larger value ensures the independence but a smaller value reduces the data size. Following the studies of Keellings and Waylen (2014, 2015) on heat waves, r is set to 4 days in this study.

Time series for the frequency, duration and intensity of warm spells were computed from the wintertime warm spell events extracted with the method presented above from Middle East temperature data (see Section 3, Data). Here, frequency is defined as the number of warm spell occurrences per winter, the duration is defined in days during a warm spell event and the intensity is defined as the maximum exceedance of the daily maximum temperature during a warm spell event. The winter period is defined here as the period during the months November through March (NDJFM). Figure 1 presents an example of the daily quantile-threshold approach used to identify warm spells in the study region for the winter of 2009-2010. The 2009-2010 winter was one of the warmest winters on record in the Middle East, thus representing a good benchmark for our method. Figure 1 shows in fact five main significant warm events between November 2009 and March 2010.

3. Data

3.1 Data sources

Atmospheric temperatures used in this study are obtained from the NCEP/NCAR Reanalysis (Kalnay et al., 1996). Daily maximum and minimum temperatures are available on a Gaussian grid (The latitudinal grid spacing varies to preserve equal areas and is approximately equal to 1.9° while the longitudinal spacing is 1.875°). Data are obtained for the period 1948-2016 for grid points over the Middle East and for the extended winter season (November to March, NDJFM).

AMO is defined as the anomaly of the area weighted average of the SST over the North Atlantic (between 0-70°N, (Trenberth and Shea, 2006; Peings and Magnusdottir, 2014; Enfield et al., 2001)). It can be obtained from the NOAA Physical Science Division at https://www.esrl.noaa.gov/psd/data/timeseries/AMO/. NAO is based on the surface sea-level pressure difference between the Subtropical (Azores) High and the Subpolar Low. NAO is obtained from the Climate Prediction Center (CPC) at the National Centers for Environmental Prediction (NCEP) at the address: http://www.cpc.ncep.noaa.gov/data/teledoc/nao.shtml. NAO is available from 1950 and AMO from 1948, and both indices are updated monthly.

3.2 Spatial extent

To compute the regional warm spell variables, the daily local maximum and minimum temperatures were averaged over a homogenous region. The definition of the homogenous region for this study is based on the EOF analysis of the winter mean temperature (Abatzoglou et al., 2009; Conroy and Overpeck, 2011). The EOF of the mean temperature during the wet season (NDJFM) for the grid points between 10-45°N and 20-65°E were extracted and the orthogonal varimax rotation was applied to the significant EOFs. Rotation of the eigenvectors is usually performed on a subset of the original EOFs in studies using EOF for the identification of the regional patterns of climate variability (White et al., 1991; Fovell and Fovell, 1993; Comrie and Glenn, 1998; Simpson et al., 2005; Abatzoglou et al., 2009; Conroy and Overpeck, 2011). Rotation allows to enhance physical interpretation. The first four principal components were tested for significance on the basis of the scree test (Cattell, 1966). The scree test is a simple method consisting in plotting the eigenvalues versus the rank and identifying changes in slope.

There are several methods to identify statistically homogeneous regions using EOFs. They can be defined, for example, by using contours (Comrie and Glenn, 1998), the maximum loading rule (Conroy and Overpeck, 2011) or cluster analysis (Guttman, 1993). Figure 2 presents the region of interest obtained with each one of these methods. They all lead to similar results, highlighting a homogenous region embracing most of the Arabian Peninsula, Levant countries, Turkey, Iraq and Iran. The region delineated using the contour defines the homogenous region used in this study.

4. Results

4.1 Trend and change point analysis

The presence of potential trends and abrupt changes in warm spell characteristics is investigated in this subsection. Specifically, abrupt changes were investigated with a Bayesian multiple change point detection procedure (Seidou et al., 2007; Seidou and Ouarda, 2007). This procedure allows to automatically detect multiple shifts or changes in the trend. The change point detection procedure was applied to the frequency of warm spells and to the following other annual variables computed from the warm spell variables: total duration, mean duration, longest duration, mean intensity and maximum intensity. Annual time series and linear trends for the various delineated segments are presented in Figure 3. A change point is detected in all cases during the late 1960s except for the mean intensity. Such a shift is coherent with the shift observed during the same period in the characteristics of global atmospheric circulation by Baines and Folland (2007). These authors highlighted how, in particular, such shift was evident in Greenland annual mean temperature patterns, eventually leading to similar changes in SST in the higher latitudes of the North Atlantic. The main cause of the late 1960s climate shift could also be found in the North Atlantic, and derives from a reduction in the northward oceanic heat flux from the North Atlantic thermohaline circulation in the 1950s to 1970s. For all variables with a change point during the late 1960s, trends have since increased.

Trends in the model parameters λ_t, p_t and σ_t are analyzed here as these parameters allow to infer on trends in the frequency, duration and intensity of warm spells. In Figure 4, trends in the model parameters λ_t, p_t and σ_t before and after the year 1967 are also superimposed on the graphs of the time series of warm spell frequency, duration and intensity respectively. The year 1967 is selected to represent the shift observed in the heat spell features during the late 1960s and corresponds to the shift obtained for the warm spell frequency with the change point detection procedure (see Figure 3a). To compute trends in the model parameters, the nonstationary POI, GEO and GP models with Time used as a covariate are fitted to the time series before and after the shift. Increasing trends are observed in the time series, since the shifts are observed, for every warm spell variable, and these trends are found to be statistically significant based on the deviance statistic. It is also worth noting that the longest warm spell happened during the winter season of 2015-2016, which is the last year of record, and the most intense warm spell occurred during the winter season of 2007-2008, to coincide with one of the most extended and intense mega-droughts on record over the region (Barlow et al., 2016; Gleick, 2014).

4.2 Validation of the probability functions

In this subsection, the choices of the different probability functions used to model warm spell variables are validated. Figure 5 compares the theoretical probability distributions inferred from data with the corresponding observed relative frequencies for the frequency, duration and intensity of winter warm spells. These graphs suggest that the selected theoretical probability distributions are suitable to model the warm spell variables. To confirm the suitability of the selected theoretical distributions, Figure 6 presents the L-moment ratio diagram with the location of the sample L-moments of the variables' duration and intensity. The sample L-moments of the duration and intensity are located respectively near the theoretical curve of the GP and the theoretical point of the exponential distribution (the continuous probability distribution analogous to the GEO). The sample L-moments of the frequency are not shown in the diagram because the POI theoretical distribution is not usually represented in moment ratio diagrams, and therefore there is missing information in the literature about the location of this distribution.

4.3 Relationship of warm spell variables with climate indices

Relationships of climate indices with the warm spell variables are evaluated in this subsection. Table 1 presents the correlations between the warm spell variables and the covariates Time, NAO and AMO. The majority of the variables are significantly correlated with NAO and AMO. Correlations with Time are weak in general except for the intensity and the mean and annual maximum intensity. However, the extended period of high values observed in the series prior to the shift during the late 1960s masks the positive significant trends observed after the shift.

Figure 7 reports on the same graph the frequency of warm spells, the inverse of the standardized wintertime NAO and the standardized wintertime AMO. Correlations between the climate indices and the frequency are clearly visible. For instance, the prolonged period of high frequency of 1950-1966 corresponds to a prolonged period of higher than normal AMO and the prolonged period of low frequency of 1967-1977 corresponds to a prolonged period of lower than normal AMO, pointing out a clear multidecadal signature in the time evolution of Middle Eastern winter warm spells. The correlation between the two climate indices for wintertime is rather weak with a value of -0.16 during the record period. This low value implies that these two covariates can be included together in a nonstationary model and improve the goodness-of-fit compared to models using the climate indices separately.

4.4 Nonstationary modelling

The nonstationary models presented in Section 2.2 were applied to the regionally averaged time series of warm spell characteristics including each one of the selected covariates, all the combinations of two covariates and the three selected covariates together. The analyses were applied to the period 1950-2016 for which both climate indices are available. Table 2 presents the optimal models obtained according to the test of the deviance for each warm spell variable and each possible configuration of the covariates. The values of the AIC statistic obtained for each optimal model are also presented and are used to compare goodness-of-fits. Here, we can observe that the goodness-of-fit obtained for models with one or more covariates is systematically higher than the one for the stationary model for a given variable. For models including one covariate, best fits are obtained with AMO for the frequency, NAO for the duration and Time for the intensity. This suggests that the climate indices have more impact on the frequency and the duration than the temporal trend, while the temporal trend has more impact on the intensity than the climate indices. From a climate dynamics point of view, this is like saying that large-scale climate oscillations basically pose the conditions to trigger the onset of winter warm spells, while the intensity of the different events may be determined by more local processes like land-atmosphere interactions and feedbacks.

For models including two covariates, the overall best goodness-of-fit statistic is obtained with NAO+AMO for the frequency, and NAO+Time for the duration and the intensity. Adding Time to either NAO or AMO (NAO+Time or AMO+Time) does not improve the corresponding model which includes only NAO or AMO for the frequency. For the duration, adding Time to NAO improves the goodness-of-fit while it is not the case for AMO+Time. For the intensity, a larger impact on the goodness-of-fit with NAO+Time than with AMO+Time is observed, where the AIC value passes from 266.58 to 248.27 for NAO+Time compared to NAO only. For the intensity, models that include Time (NAO+Time or AMO+Time) outperform models that include only one climate index (NAO and AMO) and the model including both climate indices (NAO+AMO). This result indicates that there is a strong temporal trend in the intensity which is not explained by the climate indices. Including both NAO and AMO (NAO+AMO) in a model generally improves the goodness-of-fit compared to models using each climate index separately.

This implies that both indices are somehow complementary and that it is of interest to use both indices together. Using the three covariates together (NAO+AMO+Time) leads to models with some of the best goodness-of-fit statistics for each variable: the third, the first and the second overall best ranks are obtained respectively for the frequency, duration and intensity.

It can be concluded from these results that the variability in the warm spell variables is partly explained by climate indices. The temporal trend associated with the global warming has also a great impact on the variability of the variables and this is particularly true for the intensity. The fact that the inclusion of Time with AMO has a weaker influence on the goodness-of-fit than the inclusion of Time with NAO is probably caused by the positive trend observed in AMO since the 1970s, and is coherent with global warming (see Figure 7). Indeed, it is known that AMO is a combination of a forced global warming trend with a distinct local multidecadal oscillation that arose from internal variability (Ting et al., 2009).

Figure 8 illustrates the quantiles corresponding to nonexceedance probabilities p = 0.5 and 0.9 for warm spell variables obtained with the nonstationary models including one covariate. Quantiles of each variable are presented on separate graphs as a function of the covariates NAO, AMO and Time. The quantiles corresponding to frequency and duration are represented with step functions because of the discrete nature of the probability distributions POI and GEO. It is clear from Figures 8a-8f that the relationships of the quantiles with Time are rather unrealistic for the frequency and duration. The quadratic model was selected in both cases, resulting in decreasing trends during the period 1950-1970 and increasing trends during the period 1990-2015. These trends are strongly influenced by climate oscillation patterns for which no index is included in the model in this case. For the duration, there is an outlier for an event happening during the winter 2015-2016 where for the longest duration observed, the value of NAO is in the middle range.

Figures 9-11 present the quantiles corresponding to the nonexceedance probability p = 0.9 obtained with the nonstationary models including two covariates for the frequency, duration and intensity respectively. For each variable, the optimal models obtained with the three possible combinations of two covariates are graphically represented. Quantiles are illustrated in two different ways: with 2-dimensional graphs where the quantiles are represented using colors (a, c, e), and with 3-dimensional graphs (b, d, f) where the frequency is shown as a function of the two covariates. Quantiles corresponding to the frequency and duration are also represented here with step functions for the same reasons. The figures corresponding to models with both NAO and AMO illustrate well the combined effect of both climate indices: when both covariates have extreme values of opposite signs, the quantiles are extreme (either very strong or very weak). For the frequency and duration, strong relationships with climate indices and slight temporal trends are noticed in Figures 9-10. In the case of models with covariates NAO+Time, increasing temporal trends are observed, and in the case of models with covariates AMO+Time, decreasing temporal trends are observed. These decreasing temporal trends for AMO+Time are counterintuitive in a context a global warming. However, the temporal trends in models with AMO+Time are not significant for the frequency and duration as the goodness-of-fit of models with only AMO is more optimal in both cases (see Table 2). In the case of the intensity, strong relationships with climate indices in conjunction with strong positive temporal trends are noticed, in agreement with what was observed previously.

5. Conclusions

In this study, temperatures during the winter season (NDJFM) were aggregated over a homogenous region over the Middle East to obtain regional daily average minimum and maximum temperatures. Warm spell events were identified from these regionally averaged time series and the warm spell frequency, duration and intensity were obtained. To account for the nonstationarities associated with global warming and climate oscillation patterns, statistical distributions with parameters conditional on time-dependent covariates were used to model the wintertime warm spell characteristics in the region. The covariates of the model include two important climate indices, the NAO and the AMO, explaining temperature variability in the Middle East, and Time as a covariate representing the temporal trend related to global warming.

Results show that the inclusion of any one of the covariates improves the goodness-of-fit of the stationary model. For models with only one covariate, the best fit is obtained with AMO for the frequency, NAO for the duration and Time for the intensity. This may indicate that the influence of climate oscillation patterns is more important than the influence of the temporal trend for the frequency and the duration. On the other hand, the temporal trend influences the intensity more than do climate indices. Including both climate indices generally improved the goodness-of-fit as compared to the models which include only one climate index. These results advocate for the use of both climate indices at the same time. The overall best goodness-of-fits are obtained with NAO and AMO for the frequency, NAO, AMO and Time for the duration, and NAO and Time for the intensity. These results show the importance of considering the combined effect of the temporal trend caused by global warming and climate oscillation patterns in statistical models used for the prediction of extreme climatic variables.

The nonstationary statistical models used in this study can find application in a number of different fields where conditional risk management is required, such as agriculture, public health management and hydrology. For example, seasonal predictions of the diverse climate indices can be used to model warm spell quantiles. More optimal management decisions can then be made before the start of the next season based on that information.

Acknowledgments

Financial support for the present study was provided by the Natural Sciences and Engineering Research Council of Canada (NSERC). Daily temperature data used in this study comes from the NCEP/NCAR Reanalysis database and was downloaded from the NOAA's Earth System Research Laboratory (https://www.esrl.noaa.gov/psd/data/gridded/data.ncep.reanalysis.html). Sea surface temperature data comes from the Met Office Hadley Centre (downloaded at http://hadobs.metoffice.com/hadisst/). Data for the climate indices AMO and NAO is updated and available respectively from the NOAA ESRL Physical Science Division (PSD) (https://www.esrl.noaa.gov/psd/data/timeseries/AMO/) and the NCEP Climate Prediction Center (CPC) (http://www.cpc.ncep.noaa.gov/data/teledoc/nao.shtml). The authors are grateful to the Executive Editor, Dr. Jian Lu, and to two anonymous reviewers for their comments which helped improve the quality of the manuscript.

References

Abatzoglou JT, Redmond KT, Edwards LM (2009) Classification of Regional Climate Variability in the State of California. Journal of Applied Meteorology and Climatology 48:1527-1541. doi:10.1175/2009JAMC2062.1

Abaurrea J, Asín J, Cebrián AC (2015) Modeling and projecting the occurrence of bivariate extreme heat events using a non-homogeneous common Poisson shock process. Stochastic Environmental Research and Risk Assessment 29:309-322. doi:10.1007/s00477-014-0953-9

Alexander LV et al. (2006) Global observed changes in daily climate extremes of temperature and precipitation. Journal of Geophysical Research: Atmospheres 111. doi:10.1029/2005JD006290

Ashkar F, Ouarda TBMJ (1996) On some methods of fitting the generalized Pareto distribution. Journal of Hydrology 177:117-141. doi:10.1016/0022-1694(95)02793-9

Baines PG, Folland CK (2007) Evidence for a Rapid Global Climate Shift across the Late 1960s. Journal of Climate 20:2721-2744. doi:10.1175/JCLI4177.1

Barlow M, Zaitchik B, Paz S, Black E, Evans J, Hoell A (2016) A Review of Drought in the Middle East and Southwest Asia. Journal of Climate 29:8547-8574. doi:10.1175/jcli-d-13-00692.1

Basha G, Kishore P, Ratnam MV, Jayaraman A, Agha Kouchak A, Ouarda TBMJ, Velicogna I (2017) Historical and projected surface temperature over India during the 20th and 21st century. Scientific Reports 7:2987. doi:10.1038/s41598-017-02130-3

Bayentin L, El Adlouni S, Ouarda TB, Gosselin P, Doyon B, Chebana F (2010) Spatial variability of climate effects on ischemic heart disease hospitalization rates for the period 1989-2006 in Quebec, Canada. International Journal of Health Geographics 9:1-10. doi:10.1186/1476-072x-9-5

Brown SJ, Caesar J, Ferro CAT (2008) Global changes in extreme daily temperature since 1950. Journal of Geophysical Research: Atmospheres 113. doi:10.1029/2006JD008091

Cattell RB (1966) The Scree Test For The Number Of Factors. Multivariate Behavioral Research 1:245-276. doi:10.1207/s15327906mbr0102_10

Chandran A, Basha G, Ouarda TBMJ (2016) Influence of climate oscillations on temperature and precipitation over the United Arab Emirates. International Journal of Climatology 36:225-235. doi:10.1002/joc.4339

Coles S (2001) An introduction to statistical modeling of extreme values. Springer, London.

Comrie AC, Glenn EC (1998) Principal components-based regionalization of precipitation regimes across the southwest United States and northern Mexico, with an application to monsoon precipitation variability. Climate Research 10:201-215. doi:10.3354/cr010201

Conroy JL, Overpeck JT (2011) Regionalization of Present-Day Precipitation in the Greater Monsoon Region of Asia. Journal of Climate 24:4073-4095. doi:10.1175/2011jcli4033.1

Coumou D, Rahmstorf S (2012) A decade of weather extremes. Nature Climate Change 2:491-496. doi:10.1038/nclimate1452

Coumou D, Robinson A (2013) Historic and future increase in the global land area affected by monthly heat extremes. Environmental Research Letters 8:034018. doi:10.1088/1748-9326/8/3/034018

Coumou D, Robinson A, Rahmstorf S (2013) Global increase in record-breaking monthly-mean temperatures. Climatic Change 118:771-782. doi:10.1007/s10584-012-0668-1

Crane TA, Roncoli C, Hoogenboom G (2011) Adaptation to climate change and climate variability: The importance of understanding agriculture as performance. NJAS - Wageningen Journal of Life Sciences 57:179-185. doi:10.1016/j.njas.2010.11.002

Cullen HM, deMenocal PB (2000) North Atlantic influence on Tigris–Euphrates streamflow. International Journal of Climatology 20:853-863. doi:10.1002/1097-0088(20000630)20:8<853::AID-JOC497>3.0.CO;2-M

Cullen HM, Kaplan A, Arkin PA, deMenocal PB (2002) Impact of the North Atlantic Oscillation on Middle Eastern Climate and Streamflow. Climatic Change 55:315-338. doi:10.1023/a:1020518305517

Della-Marta PM, Haylock MR, Luterbacher J, Wanner H (2007) Doubled length of western European summer heat waves since 1880. Journal of Geophysical Research: Atmospheres 112. doi:10.1029/2007JD008510

Dole R et al. (2011) Was there a basis for anticipating the 2010 Russian heat wave? Geophysical Research Letters 38. doi:10.1029/2010GL046582

Donat M et al. (2014) Changes in extreme temperature and precipitation in the Arab region: long‐term trends and variability related to ENSO and NAO. International Journal of Climatology 34:581-592. doi:10.1002/joc.3707

Ebi KL, Lewis ND, Corvalan C (2006) Climate variability and change and their potential health effects in small island states: information for adaptation planning in the health sector. Environmental Health Perspectives 114:1957-1963. doi:10.1289/ehp.8429

El Adlouni S, Ouarda TBJM, Zhang X, Roy R, Bobee B (2007) Generalized maximum likelihood estimators for the nonstationary generalized extreme value model. Water Resources Research 43:W03410. doi:10.1029/2005WR004545

El Adlouni S, Ouarda TBMJ (2009) Joint Bayesian model selection and parameter estimation of the generalized extreme value model with covariates using birth-death Markov chain Monte Carlo. Water Resources Research 45:W06403. doi:10.1029/2007wr006427

Enfield DB, Mestas-Nuñez AM, Trimble PJ (2001) The Atlantic Multidecadal Oscillation and its relation to rainfall and river flows in the continental U.S. Geophysical Research Letters 28:2077-2080. doi:10.1029/2000GL012745

Erlat E, Türkeş M (2013) Observed changes and trends in numbers of summer and tropical days, and the 2010 hot summer in Turkey. International Journal of Climatology 33:1898-1908. doi:10.1002/joc.3556

Evans JP (2010) Global warming impact on the dominant precipitation processes in the Middle East. Theoretical and Applied Climatology 99:389. doi:10.1007/s00704-009-0151-8

Folland CK, Knight J, Linderholm HW, Fereday D, Ineson S, Hurrell JW (2009) The Summer North Atlantic Oscillation: Past, Present, and Future. Journal of Climate 22:1082-1103. doi:10.1175/2008jcli2459.1

Founda D, Giannakopoulos C (2009) The exceptionally hot summer of 2007 in Athens, Greece — A typical summer in the future climate? Global and planetary change 67:227-236. doi:10.1016/j.gloplacha.2009.03.013

Fovell RG, Fovell M-YC (1993) Climate Zones of the Conterminous United States Defined Using Cluster Analysis. Journal of Climate 6:2103-2135. doi:10.1175/1520-0442(1993)006<2103:czotcu>2.0.co;2

Fraisse CW et al. (2006) AgClimate: A climate forecast information system for agricultural risk management in the southeastern USA. Computers and Electronics in Agriculture 53:13-27. doi:10.1016/j.compag.2006.03.002

Freychet N, Sparrow S, Tett SFB, Mineter MJ, Hegerl GC, Wallom DCH (2018) Impacts of Anthropogenic Forcings and El Niño on Chinese Extreme Temperatures. Advances in Atmospheric Sciences 35:994-1002. doi:10.1007/s00376-018-7258-8

Furrer EM, Katz RW, Walter MD, Furrer R (2010) Statistical modeling of hot spells and heat waves. Climate Research 43:191-205. doi:10.3354/cr00924

García-Herrera R, Díaz J, Trigo R, Luterbacher J, Fischer E (2010) A review of the European summer heat wave of 2003. Critical Reviews in Environmental Science and Technology 40:267-306. doi:10.1080/10643380802238137

Gleick PH (2014) Water, Drought, Climate Change, and Conflict in Syria. Weather, Climate, and Society 6:331-340. doi:10.1175/WCAS-D-13-00059.1

Gobron N et al. (2005) The state of vegetation in Europe following the 2003 drought. International Journal of Remote Sensing 26:2013-2020. doi:10.1080/0143116042331330293

Gonzalez R, Ouarda T, Marpu P, Allam M, Eltahir E, Pearson S (2016) Water Budget Analysis in Arid Regions, Application to the United Arab Emirates. Water 8:415. doi:10.3390/w8090415

Grotjahn R et al. (2016) North American extreme temperature events and related large scale meteorological patterns: a review of statistical methods, dynamics, modeling, and trends. Climate Dynamics 46:1151-1184. doi:10.1007/s00382-015-2638-6

Guttman NB (1993) The Use of L-Moments in the Determination of Regional Precipitation Climates. Journal of Climate 6:2309-2325. doi:10.1175/1520-0442(1993)006<2309:tuolmi>2.0.co;2

Halpert MS, Ropelewski CF (1992) Surface Temperature Patterns Associated with the Southern Oscillation. Journal of Climate 5:577-593. doi:10.1175/1520-0442(1992)005<0577:stpawt>2.0.co;2

Hansen J, Ruedy R, Sato M, Lo K (2010) Global Surface Temperature Change. Reviews of Geophysics 48. doi:10.1029/2010RG000345

Horton, R.M., Mankin, J.S., Lesk, C., Coffel, E., Raymond, C., 2016. A Review of Recent Advances in Research on Extreme Heat Events. Current Climate Change Reports: 1-18. doi:10.1007/s40641-016-0042-x

Hundecha Y, St-Hilaire A, Ouarda TBMJ, El Adlouni S, Gachon P (2008) A Nonstationary Extreme Value Analysis for the Assessment of Changes in Extreme Annual Wind Speed over the Gulf of St. Lawrence, Canada. Journal of Applied Meteorology and Climatology 47:2745-2759. doi:10.1175/2008jamc1665.1

IPCC (2007) IPCC, 2007: Summary for Policymakers. In: Climate Change 2007: The Physical Science Basis. Contribution of Working Group I to the Fourth Assessment Report of the Intergovernmental Panel on Climate Change [Solomon, S., D. Qin, M. Manning, Z. Chen, M. Marquis, K.B. Averyt, M.Tignor and H.L. Miller (eds.)]. Cambridge University Press, Cambridge, United Kingdom and New York, NY, USA.

IPCC (2012) Managing the risks of extreme events and disasters to advance climate change adaptation. A special report of Working Groups I and II of the Intergovernmental Panel on Climate Change (IPCC) [Field, C. B., V. Barros, T. F. Stocker, D. Qin, D. J. Dokken, K. L.

Ebi, M. D. Mastrandrea, K. J. Mach, G.-K. PLattner, S. K. Allen, M. Tignor, and P. M. Midgley (eds.)]. Cambridge University Press, Cambridge, United Kingdom and New York, NY, USA

Jones JW, Hansen JW, Royce FS, Messina CD (2000) Potential benefits of climate forecasting to agriculture. Agriculture, Ecosystems & Environment 82:169-184. doi:10.1016/S0167-8809(00)00225-5

Kalnay E et al. (1996) The NCEP/NCAR 40-Year Reanalysis Project. Bulletin of the American Meteorological Society 77:437-471. doi:10.1175/1520-0477(1996)077<0437:TNYRP>2.0.CO;2

Karabörk MÇ, Kahya E, Karaca M (2005) The influences of the Southern and North Atlantic Oscillations on climatic surface variables in Turkey. Hydrological Processes 19:1185-1211. doi:10.1002/hyp.5560

Karl TR, Knight RW (1997) The 1995 Chicago Heat Wave: How Likely Is a Recurrence? Bulletin of the American Meteorological Society 78:1107-1119. doi:10.1175/1520-0477(1997)078<1107:TCHWHL>2.0.CO;2

Karoly D (2009) The recent bushfires and extreme heat wave in southeast Australia. Bulletin of the Australian Meteorological and Oceanographic Society 22:10-13

Katz RW, Grotjahn R (2014) Statistical methods for relating temperature extremes to Large-Scale Meteorological Patterns. US Clivar Variations 12:4-7

Katz RW, Parlange MB, Naveau P (2002) Statistics of extremes in hydrology. Advances in Water Resources 25:1287-1304. doi:10.1016/S0309-1708(02)00056-8

Keellings D, Waylen P (2014) Increased risk of heat waves in Florida: Characterizing changes in bivariate heat wave risk using extreme value analysis. Applied Geography 46:90-97. doi:10.1016/j.apgeog.2013.11.008

Keellings D, Waylen P (2015) Investigating teleconnection drivers of bivariate heat waves in Florida using extreme value analysis. Climate Dynamics 44:3383-3391. doi:10.1007/s00382-014-2345-8

Khaliq MN, Ouarda TBMJ, Gachon P, Sushama L (2011) Stochastic modeling of hot weather spells and their characteristics. Climate Research 47:187-199. doi:10.3354/cr01003

Khaliq MN, Ouarda TBMJ, Ondo JC, Gachon P, Bobée B (2006) Frequency analysis of a sequence of dependent and/or non-stationary hydro-meteorological observations: A review. Journal of Hydrology 329:534-552. doi:10.1016/j.jhydrol.2006.03.004

Kharin VV, Zwiers FW (2005) Estimating Extremes in Transient Climate Change Simulations. Journal of Climate 18:1156-1173. doi:10.1175/JCLI3320.1

Kumar KN, Molini A, Ouarda TBMJ, Rajeevan MN (2017) North Atlantic controls on wintertime warm extremes and aridification trends in the Middle East. Scientific Reports 7:12301. doi:10.1038/s41598-017-12430-3

Kyselý J, Picek J, Beranová R (2010) Estimating extremes in climate change simulations using the peaks-over-threshold method with a non-stationary threshold. Global and planetary change 72:55-68. doi:10.1016/j.gloplacha.2010.03.006

Lang M, Ouarda TBMJ, Bobée B (1999) Towards operational guidelines for over-threshold modeling. Journal of Hydrology 225:103-117. doi:10.1016/S0022-1694(99)00167-5

Laurent C, Parey S (2007) Estimation of 100-year-return-period temperatures in France in a non-stationary climate: Results from observations and IPCC scenarios. Global and planetary change 57:177-188. doi:10.1016/j.gloplacha.2006.11.008

Lee T, Ouarda TBMJ (2011) Prediction of climate nonstationary oscillation processes with empirical mode decomposition. Journal of Geophysical Research: Atmospheres 116:D06107. doi:10.1029/2010jd015142

Lelieveld J, Proestos Y, Hadjinicolaou P, Tanarhte M, Tyrlis E, Zittis G (2016) Strongly increasing heat extremes in the Middle East and North Africa (MENA) in the 21st century. Climatic Change 137:245-260. doi:10.1007/s10584-016-1665-6

Lowe D, Ebi KL, Forsberg B (2011) Heatwave Early Warning Systems and Adaptation Advice to Reduce Human Health Consequences of Heatwaves. International Journal of Environmental Research and Public Health 8:4623. doi:10.3390/ijerph8124623

Mann ME (2002) Large-Scale Climate Variability and Connections with the Middle East in Past Centuries. Climatic Change 55:287-314. doi:10.1023/a:1020582910569

Marshall J et al. (2001) North Atlantic climate variability: phenomena, impacts and mechanisms. International Journal of Climatology 21:1863-1898. doi:10.1002/joc.693

Masselot P, Chebana F, Bélanger D, St-Hilaire A, Abdous B, Gosselin P, Ouarda TBMJ (2018) Aggregating the response in time series regression models, applied to weather-related cardiovascular mortality. Science of The Total Environment 628-629:217-225. doi:10.1016/j.scitotenv.2018.02.014

Masselot P, Chebana F, Ouarda TBMJ, Bélanger D, St-Hilaire A, Gosselin P (2018) A new look at weather-related health impacts through functional regression. Scientific Reports 8:15241. doi:10.1038/s41598-018-33626-1

Mondal A, Mujumdar PP (2015) Modeling non-stationarity in intensity, duration and frequency of extreme rainfall over India. Journal of Hydrology 521:217-231. doi:10.1016/j.jhydrol.2014.11.071

Naizghi MS, Ouarda TBMJ (2017) Teleconnections and analysis of long-term wind speed variability in the UAE. International Journal of Climatology 37:230-248. doi:10.1002/joc.4700

Nasri B, El Adlouni S, Ouarda TBMJ (2013) Bayesian Estimation for GEV-B-Spline Model. Open Journal of Statistics 3:118-128. doi:10.4236/ojs.2013.32013

Niranjan Kumar K, Ouarda TBMJ, Sandeep S, Ajayamohan RS (2016) Wintertime precipitation variability over the Arabian Peninsula and its relationship with ENSO in the CAM4 simulations. Climate Dynamics:1-12. doi:10.1007/s00382-016-2973-2

Ouarda TBMJ, Charron C (2018) Nonstationary Temperature-Duration-Frequency curves. Scientific Reports 8:15493. doi:10.1038/s41598-018-33974-y

Ouarda TBMJ, Charron C, Niranjan Kumar K, Marpu PR, Ghedira H, Molini A, Khayal I (2014) Evolution of the rainfall regime in the United Arab Emirates. Journal of Hydrology 514:258-270. doi:10.1016/j.jhydrol.2014.04.032

Ouarda TBMJ, El-Adlouni S (2011) Bayesian Nonstationary Frequency Analysis of Hydrological Variables. JAWRA Journal of the American Water Resources Association 47:496-505. doi:10.1111/j.1752-1688.2011.00544.x

Ouarda, T.B.M.J., Yousef, L.A., Charron, C., 2019. Non-stationary intensity-duration-frequency curves integrating information concerning teleconnections and climate change. International Journal of Climatology, 39(4): 2306-2323. doi:10.1002/joc.5953

Parey S, Malek F, Laurent C, Dacunha-Castelle D (2007) Trends and climate evolution: Statistical approach for very high temperatures in France. Climatic Change 81:331-352. doi:10.1007/s10584-006-9116-4

Patz JA et al. (2000) The potential health impacts of climate variability and change for the United States: executive summary of the report of the health sector of the U.S. National Assessment. Environmental Health Perspectives 108:367-376

Peings Y, Magnusdottir G (2014) Forcing of the wintertime atmospheric circulation by the multidecadal fluctuations of the North Atlantic ocean. Environmental Research Letters 9:034018. doi:10.1088/1748-9326/9/3/034018

Perkins, S.E., 2015. A review on the scientific understanding of heatwaves—Their measurement, driving mechanisms, and changes at the global scale. Atmospheric Research, 164–165: 242-267. doi:10.1016/j.atmosres.2015.05.014

Perkins SE, Alexander LV (2012) On the Measurement of Heat Waves. Journal of Climate 26:4500-4517. doi:10.1175/JCLI-D-12-00383.1

Perkins SE, Alexander LV, Nairn JR (2012) Increasing frequency, intensity and duration of observed global heatwaves and warm spells. Geophysical Research Letters 39:L20714. doi:10.1029/2012GL053361

Photiadou C, Jones MR, Keellings D, Dewes CF (2014) Modeling European hot spells using extreme value analysis. Climate Research 58:193-207. doi:10.3354/cr01191

Pulwarty RS, Melis TS (2001) Climate extremes and adaptive management on the Colorado River: Lessons from the 1997–1998 ENSO event. Journal of Environmental Management 63:307-324. doi:10.1006/jema.2001.0494

Robinson PJ (2001) On the Definition of a Heat Wave. Journal of Applied Meteorology 40:762-775. doi:10.1175/1520-0450(2001)040<0762:otdoah>2.0.co;2

Russo S et al. (2014) Magnitude of extreme heat waves in present climate and their projection in a warming world. Journal of Geophysical Research: Atmospheres 119:12500-12512. doi:10.1002/2014JD022098

Seidou O, Asselin JJ, Ouarda TBMJ (2007) Bayesian multivariate linear regression with application to change point models in hydrometeorological variables. Water Resources Research 43. doi:10.1029/2005wr004835

Seidou O, Ouarda TBMJ (2007) Recursion-based multiple changepoint detection in multiple linear regression and application to river streamflows. Water Resources Research 43. doi:10.1029/2006WR005021

Sillmann J, Croci-Maspoli M, Kallache M, Katz RW (2011) Extreme Cold Winter Temperatures in Europe under the Influence of North Atlantic Atmospheric Blocking. Journal of Climate 24:5899-5913. doi:10.1175/2011JCLI4075.1

Simpson JJ, Hufford GL, Daly C, Berg JS, Fleming MD (2005) Comparing Maps of Mean Monthly Surface Temperature and Precipitation for Alaska and Adjacent Areas of Canada Produced by Two Different Methods. Arctic 58:137-161

Stefanon M, Fabio D, Drobinski P (2012) Heatwave classification over Europe and the Mediterranean region. Environmental Research Letters 7:014023

Strupczewski WG, Singh VP, Feluch W (2001) Non-stationary approach to at-site flood frequency modelling I. Maximum likelihood estimation. Journal of Hydrology 248:123-142. doi:10.1016/S0022-1694(01)00397-3

Sun Y et al. (2014) Rapid increase in the risk of extreme summer heat in Eastern China. Nature Climate Change 4:1082-1085. doi:10.1038/nclimate2410

Sutton RT, Norton WA, Jewson SP (2000) The North Atlantic Oscillation—what role for the Ocean? Atmospheric Science Letters 1:89-100. doi:10.1006/asle.2000.0021

Thiombiano AN, El Adlouni S, St-Hilaire A, Ouarda TBMJ, El-Jabi N (2017) Nonstationary frequency analysis of extreme daily precipitation amounts in Southeastern Canada using a peaks-over-threshold approach. Theoretical and Applied Climatology 129:413-426. doi:10.1007/s00704-016-1789-7

Thiombiano AN, St-Hilaire A, El Adlouni S-E, Ouarda TBMJ (2018) Nonlinear response of precipitation to climate indices using a non-stationary Poisson-generalized Pareto model: case study of southeastern Canada. International Journal of Climatology 38:e875-e888. doi:10.1002/joc.5415

Ting M, Kushnir Y, Seager R, Li C (2009) Forced and Internal Twentieth-Century SST Trends in the North Atlantic. Journal of Climate 22:1469-1481. doi:10.1175/2008jcli2561.1

Trenberth Kevin E, Shea Dennis J (2006) Atlantic hurricanes and natural variability in 2005. Geophysical Research Letters 33:L12704. doi:10.1029/2006GL026894

Türkeş M, Erlat E (2003) Precipitation changes and variability in Turkey linked to the North Atlantic oscillation during the period 1930–2000. International Journal of Climatology 23:1771-1796. doi:10.1002/joc.962

Wang W, Zhou W, Li Y, Wang X, Wang D (2015) Statistical modeling and CMIP5 simulations of hot spell changes in China. Climate Dynamics 44:2859-2872. doi:10.1007/s00382-014-2287-1

White D, Richman M, Yarnal B (1991) Climate regionalization and rotation of principal components. International Journal of Climatology 11:1-25. doi:10.1002/joc.3370110102

Table 1. Correlations between warm spell variables and covariates.

Variable	Covariate		
	Time	NAO	AMO
Frequency (Events)	-0.07	**-0.27**	**0.42**
Duration (Days)	0.00	**-0.38***	**0.21***
Intensity (°C)	**0.24**	**-0.24***	0.17*
Total annual duration (Days)	-0.01	**-0.34**	**0.40**
Mean annual duration (Days)	0.02	**-0.28**	**0.40**
Longest annual duration (Days)	0.02	**-0.24**	**0.41**
Mean annual intensity (°C)	0.20	-0.22	**0.32**
Annual maximum intensity (°C)	0.20	-0.21	**0.33**

Significant correlations at $p < 5\%$ are in bold characters.

*NAO and AMO for the duration and intensity are averaged over a 3 month period centered on the month of the warm spell event. Otherwise indices are averaged over the whole winter season.

Table 2. AIC statistic for the optimal model of each configuration of covariates. Optimal models are determined based on the test of deviance.

Variable	Covariate	Number of covariates	AIC	Model
Frequency (Events)	Stationary	0	230.60	$Poi(\lambda)$
	Time	1	220.64	$Poi(\lambda_t = \exp(\beta_0 + \beta_1\text{Time} + \beta_2\text{Time}^2))$
	NAO	1	226.53	$Poi(\lambda_t = \exp(\beta_0 + \beta_1\text{NAO}))$
	AMO	1	217.55	$Poi(\lambda_t = \exp(\beta_0 + \beta_1\text{AMO}))$
	NAO+Time	2	228.29	$Poi(\lambda_t = \exp(\beta_0 + \beta_1\text{NAO} + \beta_2\text{Time}))$
	AMO+Time	2	218.90	$Poi(\lambda_t = \exp(\beta_0 + \beta_1\text{AMO} + \beta_2\text{Time}))$
	NAO+AMO	2	**215.99**	$Poi(\lambda_t = \exp(\beta_0 + \beta_1\text{NAO} + \beta_2\text{AMO}))$
	NAO+AMO+Time	3	217.98	$Poi(\lambda_t = \exp(\beta_0 + \beta_1\text{NAO} + \beta_2\text{AMO} + \beta_3\text{Time}))$
Duration (Days)	Stationary	0	515.53	$Geo(p)$
	Time	1	511.49	$Geo(p_t = \exp(\beta_0 + \beta_1\text{Time} + \beta_2\text{Time}^2))$
	NAO	1	503.92	$Geo(p_t = \exp(\beta_0 + \beta_1\text{NAO}))$
	AMO	1	511.70	$Geo(p_t = \exp(\beta_0 + \beta_1\text{AMO}))$
	NAO+Time	2	502.73	$Geo(p_t = \exp(\beta_0 + \beta_1\text{NAO} + \beta_2\text{Time}))$
	AMO+Time	2	513.70	$Geo(p_t = \exp(\beta_0 + \beta_1\text{AMO} + \beta_2\text{Time}))$
	NAO+AMO	2	501.31	$Geo(p_t = \exp(\beta_0 + \beta_1\text{NAO} + \beta_2\text{AMO}))$
	NAO+AMO+Time	3	**500.64**	$Geo(p_t = \exp(\beta_0 + \beta_1\text{NAO} + \beta_2\text{AMO} + \beta_3\text{Time}))$
Intensity (°C)	Stationary	0	267.93	$GP(u, \sigma, \kappa)$
	Time	1	256.43	$GP(u, \sigma_t = \exp(\beta_0 + \beta_1\text{Time}), \kappa)$
	NAO	1	266.58	$GP(u, \sigma_t = \exp(\beta_0 + \beta_1\text{NAO}), \kappa)$
	AMO	1	264.94	$GP(u, \sigma_t = \exp(\beta_0 + \beta_1\text{AMO}, \kappa))$
	NAO+Time	2	**248.27**	$GP(u, \sigma_t = \exp(\beta_0 + \beta_1\text{NAO} + \beta_2\text{Time}), \kappa)$
	AMO+Time	2	256.16	$GP(u, \sigma_t = \exp(\beta_0 + \beta_1\text{AMO} + \beta_2\text{Time}), \kappa)$
	NAO+AMO	2	265.03	$GP(u, \sigma_t = \exp(\beta_0 + \beta_1\text{NAO} + \beta_2\text{AMO}), \kappa)$
	NAO+AMO+Time	3	248.70	$GP(u, \sigma_t = \exp(\beta_0 + \beta_1\text{NAO} + \beta_2\text{AMO} + \beta_3\text{Time}), \kappa)$

Overall best AIC values are in bold characters.

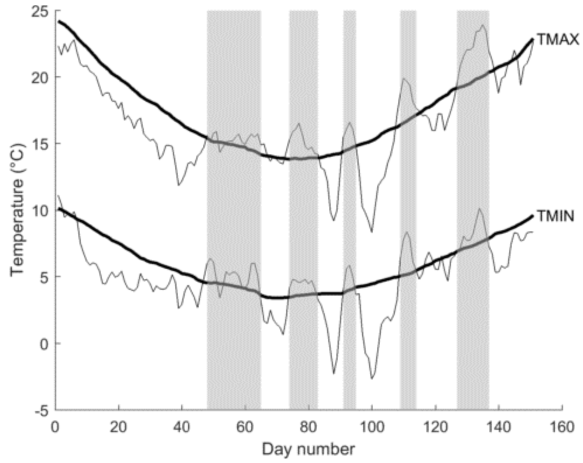

Figure 1. Warm spell occurrence (shaded area) during winter 2009-2010: Daily maximum (TMAX) and minimum temperatures (TMIN) for the winter 2009-2010 are shown in gray (light line); the black bold line represents the 90th percentiles of TMAX and TMIN

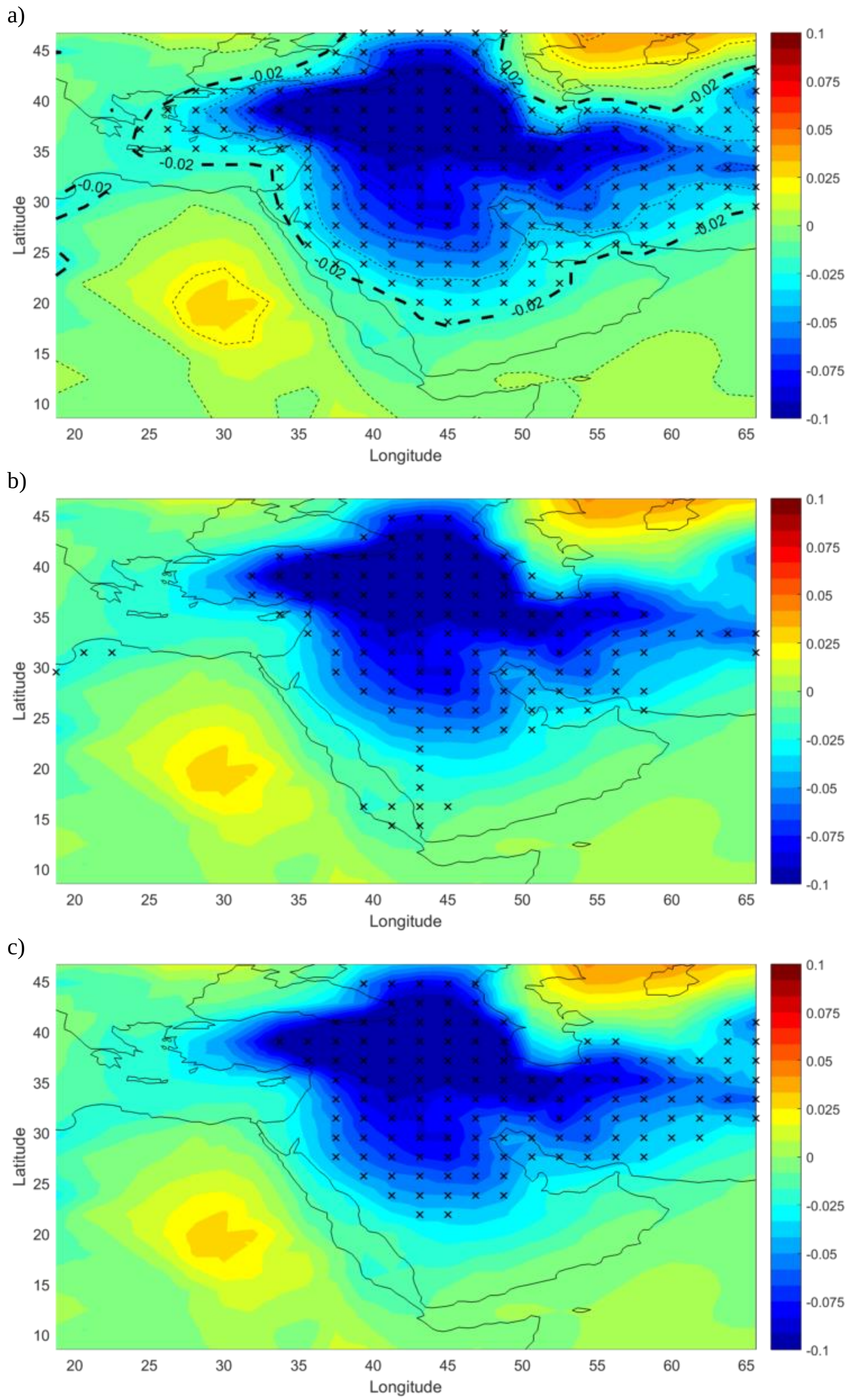

Figure 2. First rotated EOF of the mean winter temperature from the NCEP/NCAR reanalysis over the Middle East. Crosses represent the spatial distribution of grid points inside the region of interest based on contour (a), maximum loading (b) and cluster analysis (c) respectively. The black dashed line in panel 1a represents the contour line delineating the homogenous region.

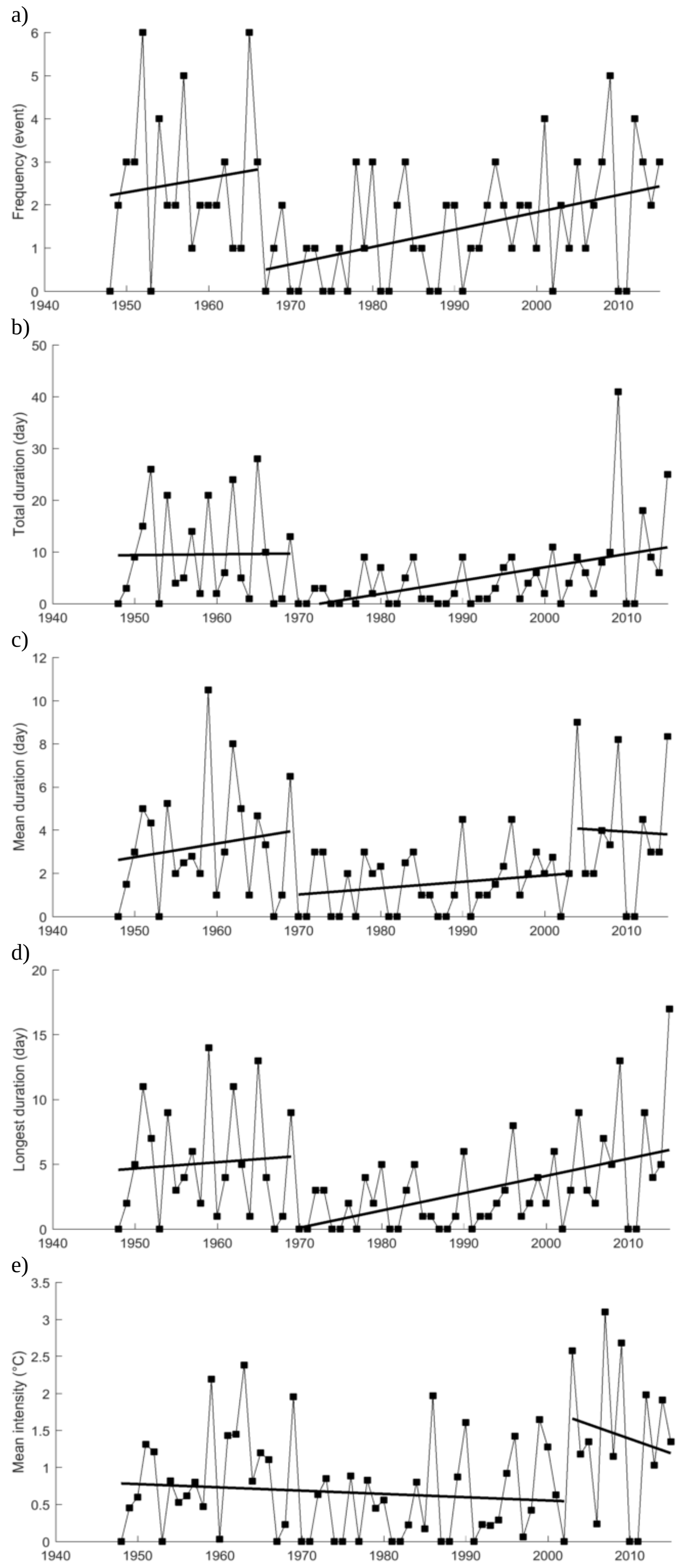

a)
Frequency (event)
b)
Total duration (day)
c)
Mean duration (day)
d)
Longest duration (day)
e)
Mean intensity (°C)

f)

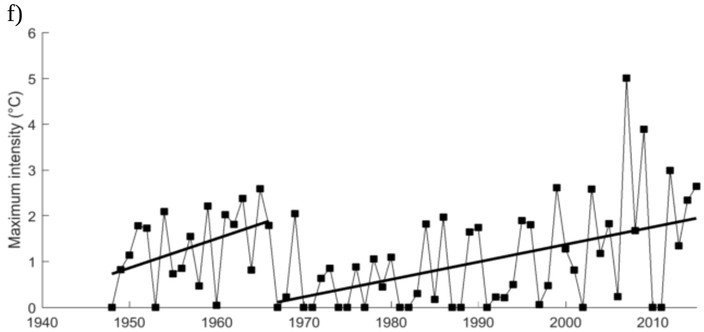

Figure 3. Trend changes in the warm spells annual time series: frequency (a), total duration (b), mean duration (c), longest duration (d), mean intensity (e) and maximum intensity (f).

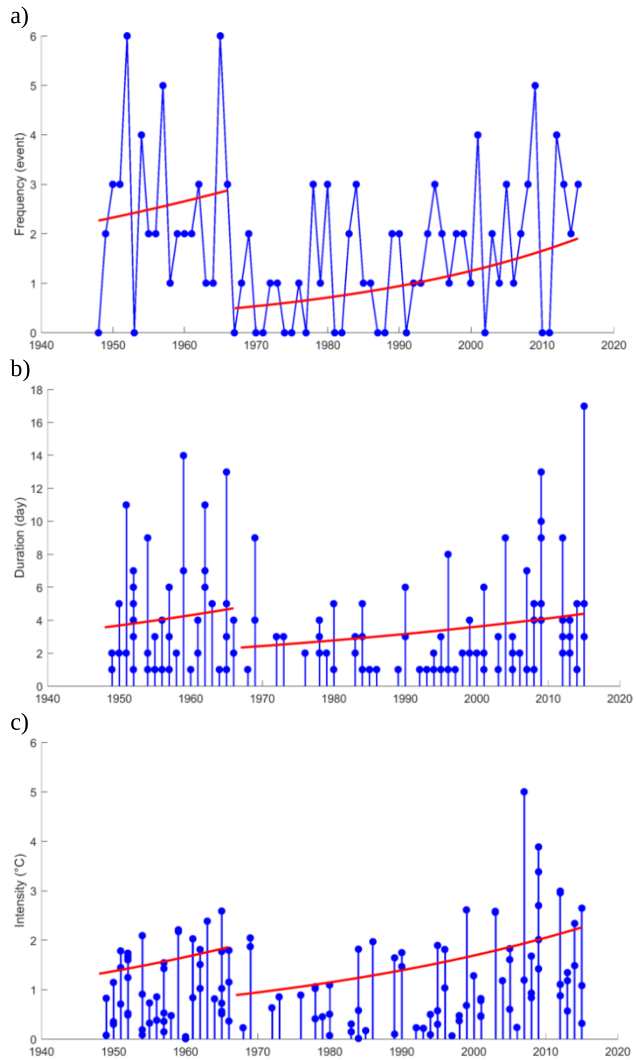

Figure 4. Frequency (a), duration (b) and intensity (c) of the regional warm spells. Trends in the theoretical distribution parameters λ_t, p_t and σ_t are reported in red.

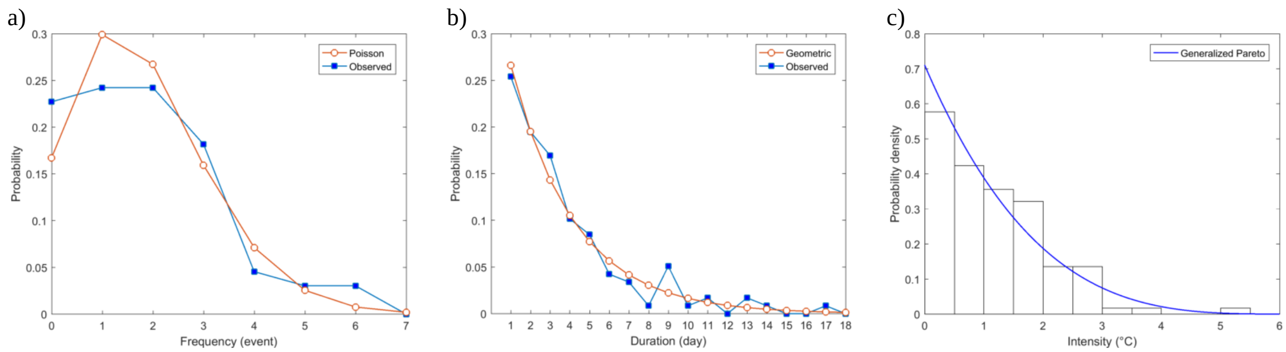

Figure 5. Observed relative frequencies and theoretical fitted models for the frequency (a), duration (b) and intensity (c) of Middle Eastern winter warm spells.

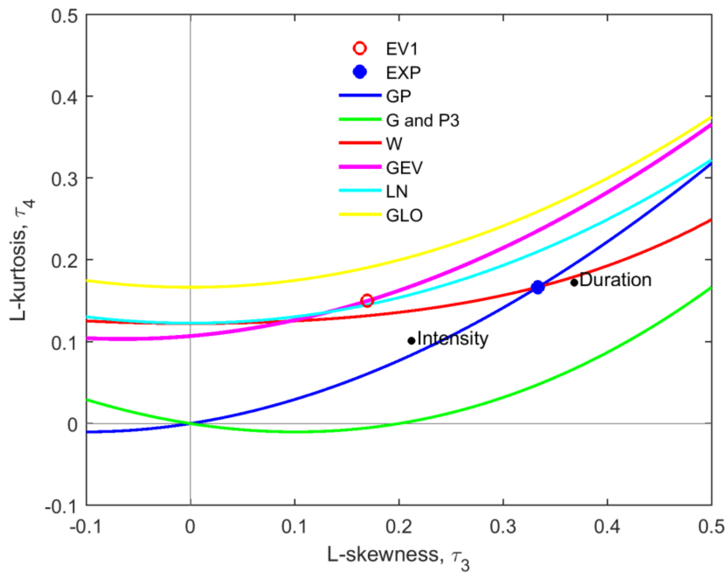

Figure 6. L-Moment ratio diagram with sample L-moments of frequency, duration and intensity. Extreme Value type I (EV1), Exponential (EXP), Generalized Pareto (GP), Gamma (G), Pearson type III (P3), Weibull (W), Generalized Extreme Value (GEV), Lognormal (LN) and Generalized Logistic (GLO).

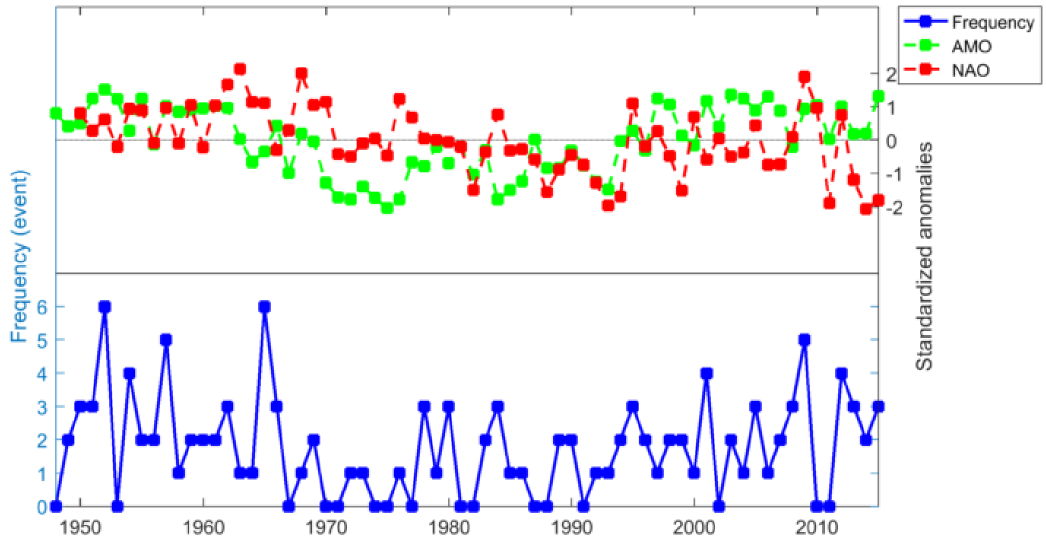

Figure 7. Frequency of warm spells (blue line and markers) and covariates NAO (red) and AMO (green) time series.

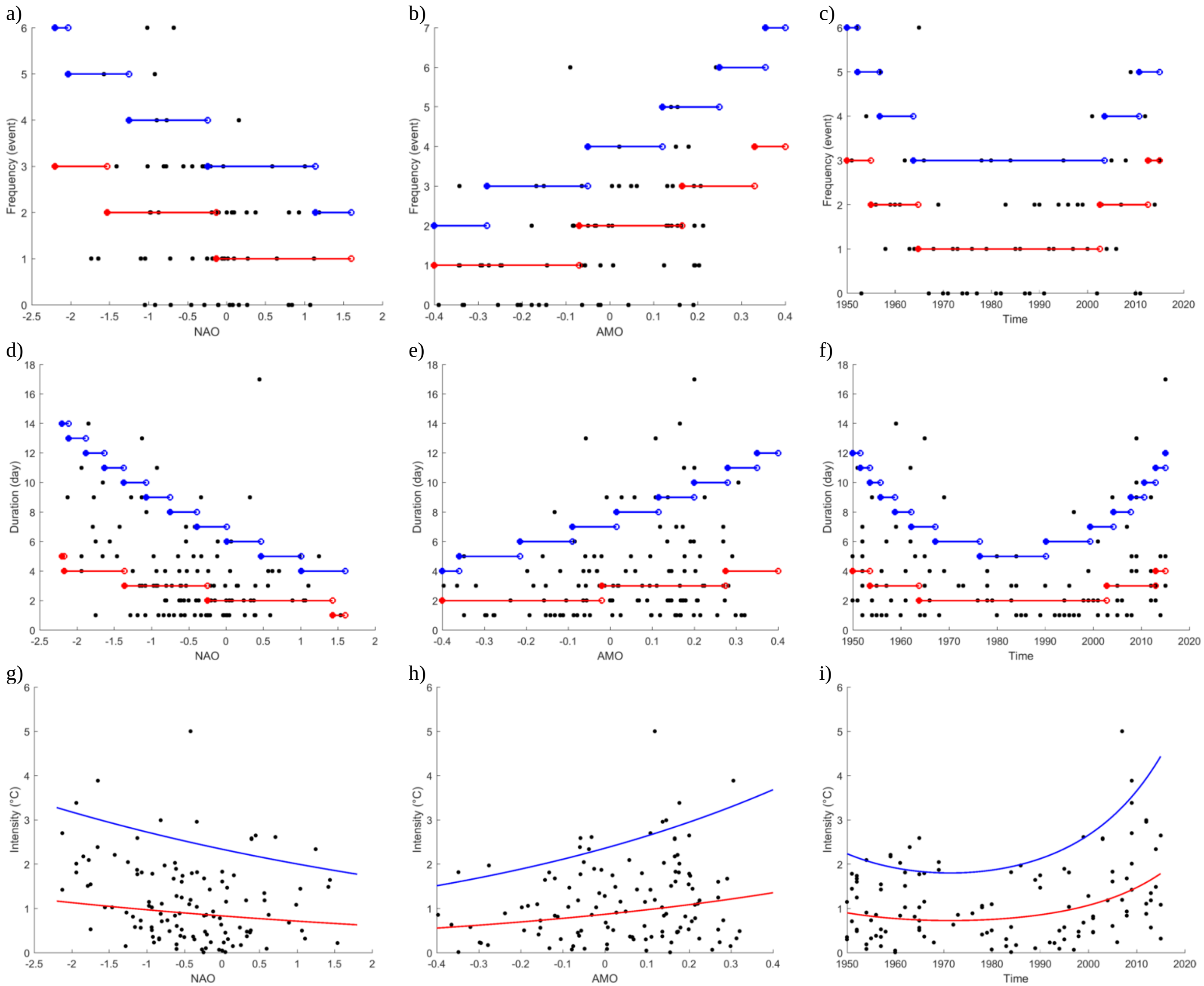

Figure 8. Quantiles corresponding to the nonexceedance probabilities p = 0.5 (red line) and 0.9 (blue line) for the frequency (a, b, c), duration (d, e, f) and intensity (g, h, i) of warm spells as a function of NAO, AMO and Time.

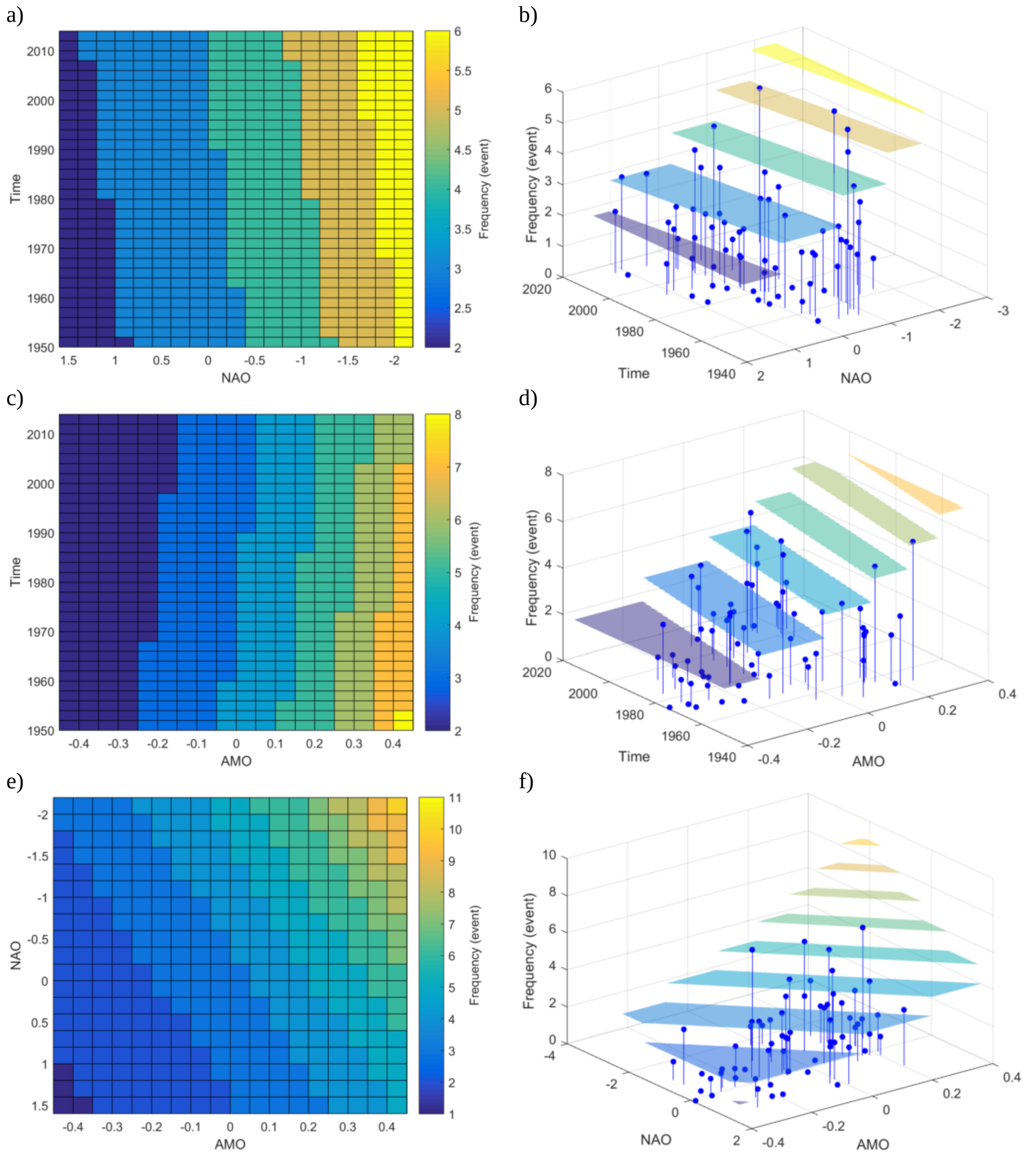

Figure 9. Quantiles corresponding to the nonexceedance probability $p = 0.9$ for the frequency as a function of NAO and Time (a,b), AMO and Time (c,d), and NAO and AMO (e,f).

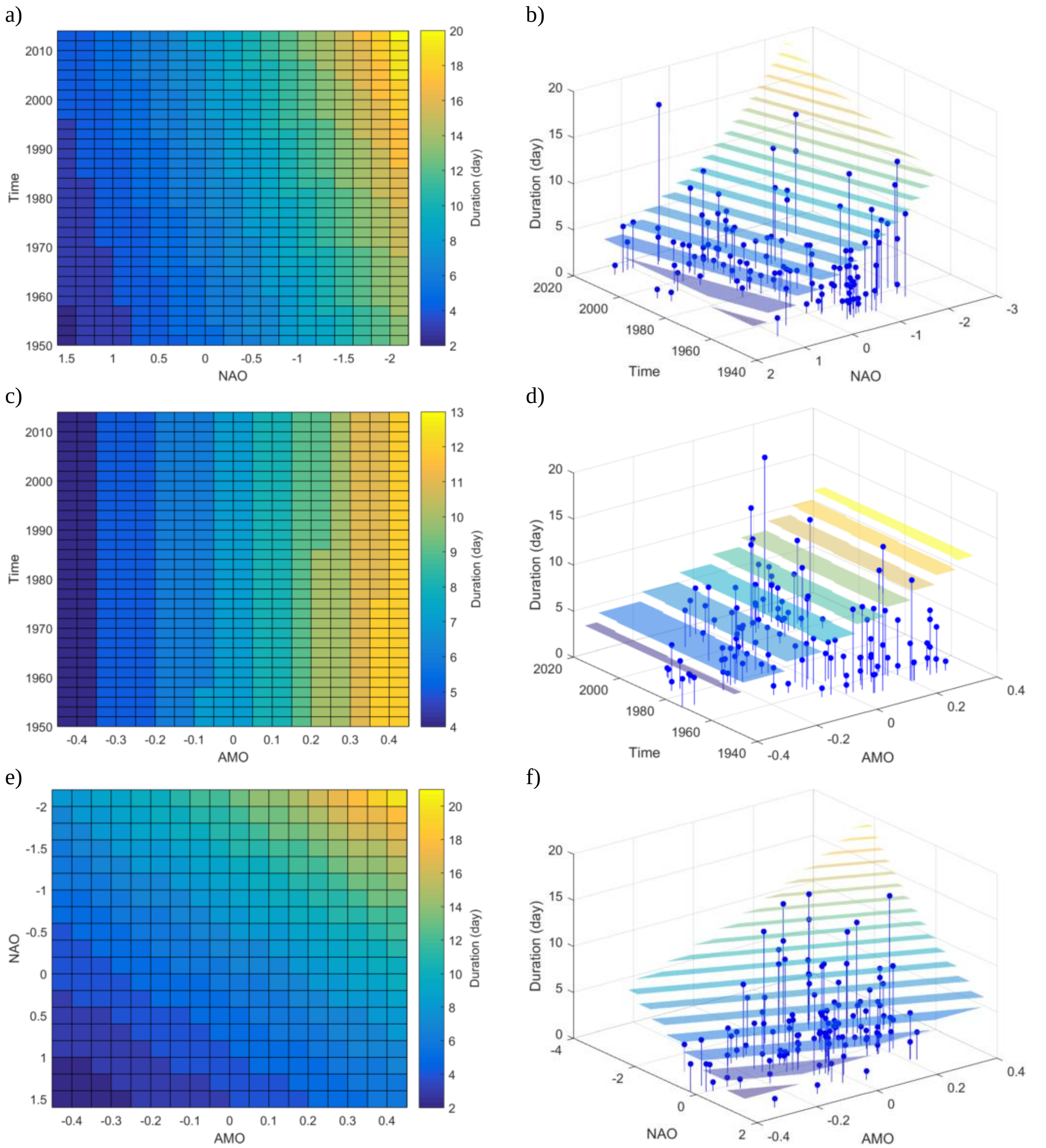

Figure 10. Quantiles corresponding to the nonexceedance probability p = 0.9 for the duration as a function of NAO and Time (a,b), AMO and Time (c,d), and NAO and AMO (e,f).

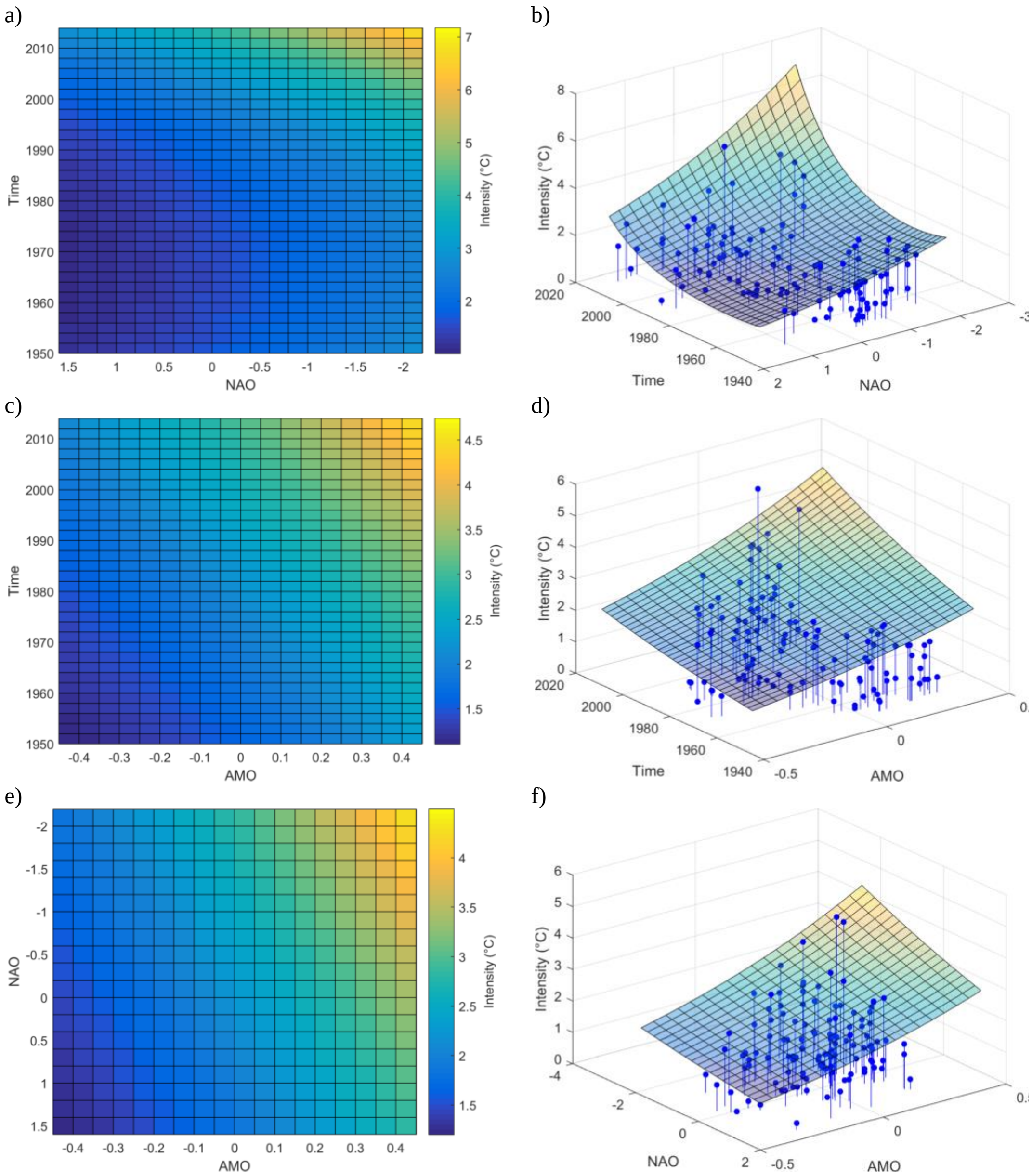

Figure 11. Quantiles corresponding to the nonexceedance probability p = 0.9 for the intensity as a function of NAO and Time (a,b), AMO and Time (c,d), and NAO and AMO (e,f).